10788 *Inorg. Chem.* **2010**, *49*, 10788–10797
DOI: 10.1021/ic101804m

Inorganic Chemistry
Article

Complex Alloys Containing Double-Mackay Clusters and $(Sb_{1-\delta}Zn_{\delta})_{24}$ Snub Cubes Filled with Highly Disordered Zinc Aggregates: Synthesis, Structures, and Physical Properties of Ruthenium Zinc Antimonides

Ding-Bang Xiong,*,†,§ Yufeng Zhao,⊥ Walter Schnelle,‡ Norihiko L. Okamoto,§ and Haruyuki Inui§

†*Department of Chemistry and Center of Material Sciences, Philipps University Marburg, Hans-Meerwein-Strasse, 35032 Marburg, Germany,* ⊥*Department of Chemical Engineering, Yanshan University, Qinhuangdao 066004, China,* ‡*Max Planck Institute for Chemical and Physics of Solids, Nöthnitzer Strasse 40, 01187 Dresden, Germany, and* §*Department of Materials Science and Engineering, Kyoto University, Kyoto 606-8501, Japan*

Received May 26, 2010

A series of cluster-based ruthenium zinc antimonides with a large unit cell were obtained. Their structures were solved by the single crystal X-ray diffraction methods. They crystallize in the cubic space group of $Fm\bar{3}c$ (No. 226) with cell dimensions of 25.098(3), 24.355(3), 24.307(3), and 24.376(3) Å for $Ru_{26}Sb_{24}Zn_{67}$ (**CA**), $Ru_{13}Sb_{12}Zn_{83.4}$ (**CB**), $Ru_{13}Sb_{6.29}Zn_{91.56}$ (**CC**), and $Ru_{13}Sb_{17.1}Zn_{74.8}$ (**CD**), respectively. By all indications, compounds **CA** and **CB** are two phases showing pronounced distinctions regarding compositions, lattice parameters, thermal and transport properties, but they are not members of an extended solid solution. Compounds **CB**, **CC**, and **CD** are three members of a same solid solution. Topologically, these four compounds contain face-centered cubic packing of double-Mackay type clusters and $(Sb_{1-\delta}Zn_{\delta})_{24}$ snub cubes filled with highly disordered zinc aggregates, with or without glue atoms between them. Both phases **CA** and **CB** are diamagnetic. There is a difference of ~170 K between their thermally stable temperatures. **CA** exhibits rather low thermal conductivity with the value of ~0.9 W m^{-1} K^{-1} at room temperature, which is about one-third that of **CB**. The electrical resistivity of **CB** is almost temperature independent. The Seebeck coefficient of **CB** is small and negative, while that of **CA** exhibits a complicated temperature dependence and undergoes a transition from p- to n-type conduction around room temperature.

Introduction

Complex alloys or complex metallic alloys (CMAs) are intermetallic compounds with large unit cells comprising from tens up to thousands of atoms.[1,2] The most prominent examples of complex alloys are cubic $NaCd_2$ with 1152 atoms per unit cell,[3] cubic β-Mg_2Al_3 with 1168 atoms,[4] and Cd_4Cu_3 (or $Cd_{160}Cu_{121}$) with about 1124 atoms.[5] The largest unit cell reported so far is tantalum copper aluminides, $Al_{55.4}Cu_{5.4}Ta_{39.1}$, with Pearson symbol $cF23256 - x$.[6] The structures of these representative examples reflect another characteristic of complex alloys: the presence of well-defined atomic clusters, frequently of pseudo icosahedral symmetry. The structures of complex alloys thus usually show duality: on the scale of several nanometers, they exhibit a periodic long-range order of clusters, whereas on a shorter scale, they could locally resemble the short-range order structure of quasicrystals or quasiperiodic crystals (QCs). The incompatibility between the well-defined long-range order and the icosahedral cluster substructure usually results in the third characteristic of complex alloys, namely, the occurrence of inherent disorder in the ideal structure. The coupling of these two competing physical length scales may have a significant impact on their physical properties, such as the electronic structure and lattice dynamics. On this basis, complex alloys are expected to exhibit remarkable transport properties, such as a combination of

*To whom correspondence should be addressed. E-mail: xiong.dingbang@ky8.ecs.kyoto-u.ac.jp.

(1) Urban, K.; Feuerbacher, M. *J. Non-Cryst. Solids* **2004**, *334−335*, 143.
(2) Dubois, J. M. An Introduction to Complex Metallic Alloys and to the CMA Network of Excellence. In *Book Series on Complex Metallic Alloys Vol. 1: Basics of Thermodynamics and Phase Transitions in Complex Intermetallics*; Belin-Ferré, E., Ed.; World Scientific: Singapore, 2008; pp 1−29.
(3) Pauling, L. *Amer. Sci.* **1955**, *43*, 285.
(4) Samson, S. *Acta Crystallogr.* **1965**, *19*, 401.
(5) Samson, S. *Acta Crystallogr.* **1967**, *23*, 586.
(6) Weber, T.; Dshemuchadse, J.; Kobas, M.; Conrad, M.; Harbrecht, B.; Steurer, W. *Acta Crystallogr., Sect. B* **2009**, *65*, 308.
(7) Maciá, E. *Phys. Rev. B* **2009**, *79*, 245112.
(8) Smontara, A.; Smiljanić, I.; Bilušić, A.; Jaglićić, Z.; Klanjšek, M.; Roitsch, S.; Dolinšek, J.; Feuerbacher, M. *J. Alloys Compd.* **2007**, *430*, 29.
(9) (a) Snyder, G. J.; Toberer, E. S. *Nat. Mater.* **2008**, *7*, 105. (b) Kauzlarich, S. M.; Brown, S. R.; Snyder, G. J. *Dalton Trans.* **2007**, 2099. (c) Brown, S. R.; Kauzlarich, S. M.; Gascoin, F.; Snyder, G. J. *Chem. Mater.* **2006**, *18*, 1873. (d) Kleinke, H. *Chem. Mater.* **2010**, *22*, 604.
(10) Allio, C.; Harbrecht, B. *Z. Anorg. Allg. Chem.* **2006**, *632*, 2142.

 Published on Web 10/28/2010

Table 1. Summary of Nominal Compositions, Products, and Refined Lattice Parameters for Complex Alloys in Ru−Sb−Zn System

	proportion (%)		(lattice parameters in Å)[c]		
reaction	Ru/Sb/Zn (T.P.[a])	main phases and estimated yields[b]	powder data	single crystal data	crystals
I	25.0/18.7/56.3 (B)	30% cF_L + 60% $Ru_9Zn_7Sb_8$[d] + 10% $Ru_3Sb_{0.97}Zn_{11}$[d]	25.121(7)		
II	23.1/21.7/55.2 (B)	40% cF_L + 35% cF_S + 15% $RuSb_2$ + 20% U_1	25.133(9), 24.350 (9)		
III	22.8/21.1/56.1 (A)	> 95% cF_L	25.118(3)	**25.098(3)**	**CA**
IV	19.5/12.3/68.2 (B)	45% cF_L + 40% $RuZn_6$ + 15% U_2	25.131(1)		
V	19.0/16.5/64.5 (B)	50% cF_L + 35% cF_S + 15% $RuSb_2$	25.144(1), 24.344(6)	**25.181(3)**, **24.371(2)**	**CA-s1, CB-s1**
VI	19.0/16.5/64.5 (C)	60% cF_L + 25% cF_S + 5% $RuSb_2$ + 10% U_3	25.124(7), 24.344(7)		
VII	12.6/11.7/75.7 (B)	65% cF_S + 10% $RuSb_2$ + 25% U_4	24.334(8)	**24.307(3)**	**CC**
VIII	12.0/11.1/76.9 (A)	> 98% cF_S	24.347(1)	**24.355(3)**	**CB**
IX	11.8/20.0/68.2 (B)	90% cF_S + 10% U_5	24.352(2)	**24.376(3)**	**CD**
X	14.3/42.8/42.9 (B)	25% cF_S + 75% U_6	24.340(6)	**24.339(3)**	**CB-s2**

[a] Temperature Programs (T.P.) A, B, and C were described in the text. [b] cF_S and cF_L denote the cubic phases with smaller lattice parameters locating in the ranges of 24.3−24.4 Å and larger 25.1−25.2 Å, respectively. U_i (i = 1, 2, 3, 4, 5, 6) denote different unknown phases. [c] Lattice parameters from powder data were refined from the peaks within 20°−50°. Bold numbers representing lattice parameters for single crystal structures are reported in this work and coded in the last column. [d] From the reference 14.

metallic electrical conductivity with low thermal conductivity, or tunable electrical and thermal resistances by varying the composition.[7,8] Therefore, complex alloys are good places to look for improved thermoelectric materials.[9]

Initially, we noticed double-Mackay clusters $Ru_{13}Zn_{114}$ with diameter of about 1.4 nm in the binary phase $Ru_{13-\delta}Zn_{128-\delta'}$ (denoted as **HA**)[12] ($P6_3/mmc$, a = 12.943(2) Å and c = 57.552(8) Å, isostructure with $FeZn_{10}$[13]). These double-Mackay clusters are fused to each other by sharing Zn_4 squares in the *ac* plane, while they are separated by icosahedra and disordered clusters along the *c* axis with the distances between the cluster centers of about 28.7 Å. We therefore focused on the possibility to experimentally construct new complex alloys using these $Ru_{13}Zn_{114}$ double-Mackay clusters as structural units by chemical substitution in **HA** with antimony.

In this way, a series of ruthenium zinc antimonides were obtained, $Ru_{26}Sb_{24}Zn_{67}$ (**CA**), $Ru_{13}Sb_{12}Zn_{83.4}$ (**CB**), $Ru_{13}Sb_{6.29}Zn_{91.56}$ (**CC**), $Ru_{13}Sb_{17.1}Zn_{74.8}$ (**CD**), containing 839.7−935.9 atoms in the face-centered cubic unit cell with cell dimensions ranging from 24.307(3) to 25.098(3) Å. Their structures contain double-Mackay clusters[10] and novel $(Sb_{1-\delta}Zn_\delta)_{24}$ snub cubes filled with highly disordered zinc aggregates, which are analogous to the ordered phase $Mo_7Sn_{12}Zn_{40}$[11] but with different decorations. The complex structure with highly disordered parts of these compounds results in reasonably good electrical conductivity and rather low thermal conductivity.

We studied this system with three expectations: (a) to demonstrate the use of icosahedral clusters as structural units to construct novel complex alloys, (b) to introduce inherent disorder caused by icosahedral cluster substructures in a periodic crystal to create phonon scattering centers, in turn, reducing lattice thermal conductivity, and (c) to isolate some possible ternary derivatives of thermoelectric zinc antimonides.

Experimental Section

Synthesis and Phase Characterization. All samples were prepared via high-temperature reactions of Ru (Degussa, 99.9%), Zn (Chempur, 99.99%), and Sb (99.8%) in evacuated fused-silica tubes. Three temperature programs were applied: (A) The samples were heated up to 1273 K at a rate of 60 K/h and homogenized at this temperature for 5 h. Then the temperature was decreased to 873 K at a rate of 50 K/h and held for 4−5 days; (B) similar to (A), but the time for ramping and annealing were shorter than that in (A). The samples were heated up to 1273 K at a rate of 200 K/h and homogenized at this temperature for 3 h. Then the temperature was decreased to 823 K at the rate of 100 K/h and held for 3 days; (C) similar to (A), but the homogenization temperature was decreased from 1273 to 1073 K. Thereafter, the ampules were slowly cooled down to room temperature in tube furnaces. In all the reactions, the reactants were placed at the least hot site of the ampules, and the furnaces were placed on a small slope to make sure the elements contact thoroughly. Each reaction generated one single chunk, and the inside wall of the ampules was clear except for the part where the reaction took place. Therefore, the loss of Zn and Sb because of condensation outside the reaction zone was minor. All the samples are stable in air for more than two years. Table 1 summarizes loaded proportions, temperature programs, phase identities, and refined lattice parameters from both powder patterns and single crystals.

Powder X-ray diffraction patterns were recorded with an X'pert MPD diffractometer (Philips) operating in Bragg−Brentano geometry with Cu K_α radiation. A single crystalline silicon disk was used as a sample holder. Phase identification was done with the aid of STOE WinXPOW[15] and lattice parameter refinements were performed using X'Pert HighScore Plus[16] (Supporting Information, Figure S1). The lattice parameters refined from powder data were given as a comparison with those from single crystal data.

Chemical compositions of selected samples were examined in a scanning electron microscope (CS 4DV, CamScan) providing an energy dispersive X-ray spectrometer (EDS, Si(Li)-detector, Noran Instruments). No impurities of elements heavier than carbon were found to be present in the samples. The quantitative analyses confirmed the results of the single-crystal structural refinements.

Crystal Structure Characterization. Seven crystals from the samples with different nominal compositions were studied by single-crystal X-ray diffraction in this work. Four of them (**CA**, **CB**, **CC**, and **CD**), showing obvious differentiations between structures and/or compositions, are reported in the text as representatives, whereas **CA-s1**, **CB-s2**, and **CB-s3** concur with **CA** and **CB**, respectively, and their crystallographic parameters are given in the Supporting Information. The diffraction intensities were recorded with an imaging plate diffractometer (IPDS, Stoe & Cie.) operating with MoK_α (λ = 0.71069 Å)

(11) Belin, C. H. E.; Belin, R. C. H. *J. Solid State Chem.* **2000**, *151*, 85.
(12) Steurer, W.; Deloudi, S. *Acta Crystallogr., Sect. A* **2008**, *64*, 1.
(13) Hillebrecht, H.; Kuntze, V.; Gebhardt, K. *Z. Kristallogr.* **1997**, *212*, 840.
(14) (a) Xiong, D. B.; Zhao, Y. F.; Okamoto, N. L.; Pietzonka, C.; Waki, T.; Inui, H. *Inorg. Chem.* **2010**, DOI: 10.1021/ic1015669. (b) Xiong, D. B.; Yang, K.; Zhao, Y. F.; Ma, J. *Dalton Trans.* **2010**, *39*, 8331.
(15) *WinXPOW*, v. 1.2; STOE & Cie GmbH: Darmstadt, Germany, 2000.
(16) *X'Pert HighScore Plus*, v. 2.2.3; PANalytical B.B.: Almelo, The Netherlands, 2007.

Table 2. Crystallographic and Technical Data of the Single Crystal Structure Refinement of Complex Alloys in the Ru−Sb−Zn System

	CA	CB	CC	CD
formula	$Ru_{26}Sb_{24}Zn_{67}$	$Ru_{13}Sb_{12}Zn_{83.4}$	$Ru_{13}Sb_{6.29}Zn_{91.6}$	$Ru_{13}Sb_{17.1}Zn_{74.8}$
M_r	9929.6	8228.4	8055.8	8293.1
space group (no.), Z	$Fm\bar{3}c$ (226), 8			
Pearson symbol	*cF*936	*cF*867.2	*cF*888.8	*cF*839.7
a/Å	25.098(3)	24.355(3)	24.307(3)	24.376(3)
V/Å^3	15810(3)	14447(3)	14362(3)	14484(3)
D_c/g cm^{-3}	8.34	7.57	7.46	7.546
μ/mm^{-1}	32.70	34.09	34.84	33.99
θ_{max}/deg	28.12	33.09	33.00	33.10
refl. coll./R(int)	34904/0.0744	48761/0.0870	36349/0.0872	49083/0.1148
data/parameter	873/65	1226/78	1215/74	1233/68
R1/wR2 [$I_o > 2\sigma(I_o)$][a,b]	0.0295/0.0299	0.0390/0.0440	0.0591/0.0753	0.0508/0.0677
[all data]	0.0651/0.0653	0.0933/0.0968	0.1544/0.1696	0.1329/0.1422
goodness of fit (F^2)	1.253	1.144	1.085	1.057
$\Delta\rho_{min}/\Delta\rho_{max}$/e Å^{-3}	−1.797/1.878	−1.421/1.095	−2.480/2.985	−1.783/2.748

[a] $R = \sum||F_o| - |F_c||/\sum|F_o|$. [b] $wR = \{\sum w(F_o^2 - F_c^2)^2/\sum w(F_o^2)^2\}^{1/2}$.

radiation at room temperature. Numerical absorption corrections based on the sizes and shapes of the crystals were applied to the data sets with the programs of X-SHAPE[17] and X-RED.[18] Systematic absence conditions suggested two possible space groups for these data sets, $F\bar{4}3c$ and $Fm\bar{3}c$. However, the values of $|E^2 - 1|$ ranging from 0.96 to 1.0 strongly suggested that all structures were centrosymmetric, so the space groups were tentatively taken to be $Fm\bar{3}c$. All structures were successfully solved by applying a direct method and subsequently refined on F^2 with a full-matrix least-squares algorithm with the aid of the program of SHELXTL v 6.1.[19]

Ten independent sites were located in the initial structural model using a direct method in **CA**: four Sb atoms, one Ru atom, and five Zn atoms. After another residual peak with moderately strong intensity was assigned as Zn21, the $R1$ value converged at ∼7.3%. The isotropic displacement parameters for three of four Sb atoms were somewhat larger (0.011, 0.011, and 0.017 Å^2) and that for Zn21 was considerably larger (0.15 Å^2) than the average value for the others (0.008 Å^2). Subsequently these three Sb atoms were reassigned as lighter Ru atoms, and Zn21 was refined as a partially occupied site. The site occupancy factor (SOF) was checked for deviation from unity by freeing the SOF of an individual atom while the remaining SOFs were fixed. Except for Zn21 with SOF ≈ 0.64, all atoms were fully occupied allowing for 2σ standard deviations. The $R1$ value converged at ∼6% at this stage. The following anisotropic refinement resulted in $R1 \approx 4.9\%$ and additional three weak diffraction peaks in a difference Fourier map. Examination of their environments revealed that these residual peaks had short distances to Zn21 ranging from 1.01 to 2.33 Å and reasonable distances to the other sites. And then these weak peaks were assigned as Zn22, Zn23, and Zn24, and their occupancies were refined in subsequent steps to 0.12(2), 0.16(3), and 0.09(1), respectively, and the occupancy of Zn21 decreased to 0.25(3). Then the $R1$ value converged at ∼3%. Their displacement parameters ranged from 0.017 to 0.067 Å^2. Analysis of these four partially occupied Zn atoms revealed that they defined a rombicdodecahedral symmetry (Supporting Information, Figure S2). Zn21, Zn22, and Zn23 combined type-1 and type-2 disorders as found in MCd_6 (M = rare earth or Ca)[20] and Zn24 split around the 4-fold axes. Finally, the highly disordered aggregates were refined isotropically with the constraints on their displacement parameters, while other atoms were refined anisotropically. The final refined composition was in excellent agreement with the EDS results.

Similarly, a direct method gave out 10 independent sites in **CB**: 2 Sb atoms, 1 Ru atom, and 7 Zn atoms. After a few cycles of isotropic refinement, $R1$ converged at ∼12%. The SOF was checked for deviation from unity by freeing the SOF of an individual atom while the remaining SOFs were fixed. The SOFs of all the assigned Sb and Ru atoms decreased by ∼20%, and that of Zn21 decreased by ∼36%. Subsequently, the two assigned Sb atoms were reassigned as lighter Ru10 and Ru14, and Ru as Zn12, respectively, and then full SOFs were obtained for these sites allowing for 2σ standard deviations. With partially occupied Zn21, the $R1$ value converged at ∼9.8% at this stage. Analysis of the difference Fourier map suggested additional two weak diffraction peaks. Examination of their environments revealed that one position was very close (0.3 Å) to Zn17a, and the other position had a short distance (1.7 Å) to Zn21. Thus, the two weak peaks were assigned as Zn17b and Zn22, and the occupancies of Zn17a, Zn17b, Zn21, and Zn22 were refined in subsequent steps to 0.89(2), 0.28(2), 0.73(3), and 0.13(1), respectively. And then the $R1$ value converged at ∼6.2%. However, the Sb atom was missing at this stage. Checking the structural model, we found that the sum of SOFs of Zn17a and Zn17b (∼1.2) is obviously larger than unity. These two closed Zn sites were located at the fully occupied Sb sites in the structure of **CA**. Reasonably refined composition and displacement parameters were obtained if we reassigned Zn17a and Zn17b as Sb17 and Zn17, respectively. When assignment of these two sites was reversed, the displacement parameter of the Zn site (0.004 Å^2) was too low compared with the averaged value of other Zn sites (0.017 Å^2). The model with Sb/Zn mixed occupied single site was also tried and resulted in an unstable refinement, which confirmed the model with the splitting sites. At the same time, one additional very weak diffraction peak with a short distance to Zn21 (1.6 Å) was located. It was assigned as Zn30, and its occupancy was refined to 0.026. The atoms with such a low occupancy were also observed in other zinc-rich antimonides, and appeared as interstitial atoms.[21,22] Finally, least-squares refinements with anisotropic parameters converged at $R1 = 3.90\%$, $wR2 = 4.40\%$, GOF = 1.144 for 78 parameters and 1141 independent reflections ($I > 2\sigma(I)$).

The refinements on **CC** and **CD** were almost the same with **CB**. The major differences between them were the discrepancies of the atomic ratio of Sb17/Zn17 and with (**CB**) or without (**CC**, **CD**) the Zn30 atom with extremely low occupancy. Additionally,

(17) *X-SHAPE, Crystal Optimization for Numerical Absorption Correction*, v. 2.01; Sote & Cie.: Darmstadt, Germany, 2001.

(18) *X-RED, Data Reduction Program*, v. 1.02; Stoe & Cie.: Darmstadt, Germany, 2001.

(19) Sheldrick, G. M. *SHELXTL Programs*, version 6.10; Bruker AXS: Madison, WI, 1998.

(20) Pay Gómez, C.; Lidin, S. *Phys. Rev. B* **2003**, *68*, 024203.

(21) Liu, Y.; Chen, L.; Li, L. H.; Wu, L. M.; Zelinska, O. Y.; Mar, A. *Inor. Chem.* **2008**, *47*, 11930.

(22) Snyder, G. J.; Christensen, M.; Nishibori, E.; Caillat, T.; Iversen, B. B. *Nat. Mater.* **2004**, *3*, 458.

Table 3. Structure Data for Ruthenium Zinc Antimonides

cluster	shell	atom	site	*x*	*y*	*z*	SOF	U_{eq}/Å^2
Double-Mackay Cluster[a]	center	Ru10	8*b*	0[b]	0	0	1	0.0043(4)
				0	0	0	1	0.0149(3)
				0	0	0	1	0.0121(4)
				0	0	0	1	0.0127(5)
	icosahedron	Zn11	96*i*	0	0.05392(4)	0.08637(4)	1	0.00951(19)
				0	0.05612(4)	0.08925(4)	1	0.0190(2)
				0	0.05619(5)	0.08934(5)	1	0.0157(2)
				0	0.05616(6)	0.08924(6)	1	0.0170(3)
	icosidodecahedron	Zn12	48*e*	0	0	0.18024(6)	1	0.0106(3)
				0	0	0.18190(6)	1	0.0209(3)
				0	0	0.18185(8)	1	0.0174(3)
				0	0	0.18187(8)	1	0.0188(4)
		Zn13	192*j*	0.09351(3)	0.05575(3)	0.15006(3)	1	0.01070(15)
				0.09348(3)	0.05873(3)	0.14922(3)	1	0.02173(18)
				0.09349(4)	0.05885(4)	0.14928(4)	1	0.01838(19)
				0.09350(4)	0.05879(4)	0.14924(4)	1	0.0197(3)
	icosahedron	Ru14	96*i*	0	0.10157(3)	0.17089(3)	1	0.00674(14)
				0	0.11403(3)	0.17808(3)	1	0.01703(16)
				0	0.11409(3)	0.17802(3)	1	0.01400(16)
				0	0.11404(4)	0.17807(4)	1	0.0151(2)
	rhombicosi-dodecahedron	Ru15	96*i*	0	0.15118(3)	0.27940(3)	1	0.00982(14)
		Zn15	96*i*	0	0.16054(5)	0.27718(4)	1	0.0272(2)
				0	0.16064(6)	0.27711(6)	1	0.0241(3)
				0	0.16065(7)	0.27714(6)	1	0.0251(3)
		Zn16	96*h*	0.05862(3)	0.05862(3)	1/4	1	0.0114(2)
				0.06061(3)	0.06061(3)	1/4	1	0.0223(2)
				0.06068(4)	0.06068(4)	1/4	1	0.0193(2)
				0.06065(4)	0.06065(4)	1/4	1	0.0204(3)
		Sb17	192*j*	0.07632(15)	0.16707(15)	0.79431(15)	1	0.00957(9)
				0.09043(7)	0.16384(3)	0.20384(3)	0.50(5)	0.0394(11)
				0.10163(12)	0.16484(13)	0.20450(14)	0.262(4)	0.0209(6)
				0.09406(5)	0.16381(5)	0.20398(5)	0.714(6)	0.0386(4)
		Zn17	192*j*					
				0.10119(10)	0.16401(5)	0.20435(5)	0.36(8)	0.022(2)
				0.08898(7)	0.16342(2)	0.20372(9)	0.709(5)	0.0281(5)
Glue Cluster	center	Ru20	8*a*	1/4	1/4	1/4	1	0.0043(4)
		Zn20	8*a*	1/4	1/4	1/4	1	0.0305(8)
				1/4	1/4	1/4	1	0.0268(10)
				1/4	1/4	1/4	1	0.0282(11)
	disordered[c]	**CA** Zn21	64*g*	0.31044(18)	0.18956(18)	0.31044(18)	0.242(6)	0.03
		CA Zn22	192*j*	0.26281(5)	0.1871(4)	0.3292(4)	0.104(3)	0.04
		CA Zn23	192*j*	0.29023(4)	0.1899(3)	0.3234(3)	0.155(3)	0.04
		CA Zn24	192*j*	0.2414(7)	0.15488(5)	0.27266(5)	0.078(2)	0.04
		CB Zn21	48*f*	0.13566(8)	1/4	1/4	0.734(8)	0.0207(6)
		CB Zn22	192*j*	0.16454(2)	0.22872(2)	0.18911(2)	0.133(4)	0.0175(15)
		CC Zn21	48*f*	0.13555(10)	1/4	1/4	0.728(8)	0.0162(5)
		CC Zn22	192*j*	0.1648(3)	0.2290(3)	0.1890(3)	0.132(4)	0.0142(15)
		CD Zn21	48*f*	0.13555(10)	1/4	1/4	0.728(13)	0.0173(8)
		CD Zn22	192*j*	0.1644(3)	0.2288(3)	0.1889(3)	0.134(7)	0.016(2)
	Snub Cube	Sb17 and Zn17 in double-Mackay cluster						
Glue Atom		Zn30	24*d*	0	1/4	1/4		0.0134(4)
			48*f*	0.06908(3)	1/4	1/4	0.026(8)	0.026(17)
				0.069(6)	1/4	1/4	0.04(2)	0.07(4)

[a] Only the inner four shells are showed, the outermost Ru_{12} icosahedral shell is formed by Ru15 atoms from the neighboring fourth shell and omitted; [b] Structure data from the first line to the fourth line refer to compound **CA**, **CB**, **CC** and **CD**, respectively; [c] Disordered zinc in **CA** was refined with isotropic displacement parameters which were fixed.

comparing structures of **CA**, **CB**, **CC**, and **CD**, structural models with Ru/Zn mixtures or partially occupied Ru at Ru15 and Ru20 sites were also tried, resulting in either a small occupation fraction of Zn or a small deviation from unity, respectively.

Details concerning data collection, crystallographic data, and atomic coordinates are summarized in the Table 2 and Table 3. Further details on the crystal structure investigations may be obtained from the Fachinformationszentrum Karlsruhe, 76344 Eggenstein-Leopoldshafen, Germany (fax: (+49) 7247−808−666; e-mail: crysdata@fiz-karlsruhe.de), on quoting the depository number CSD-421336, CSD-421337, CSD-421338, and CSD-422100 for **CA**, **CB**, **CC**, and **CD**, respectively.

Physical Properties Measurements. The thermo-chemical properties of samples from reaction **III** and **VIII** with almost pure products were studied in the temperature range 623−1323 K employing a differential scanning calorimeter (DSC, setsys 16/18, Setaram). To suppress decomposition by possible incongruent vaporization of zinc, the cold-pressed samples (∼40 mg, 2.8 mm across) were sealed in previously outgassed, evacuated silica crucibles which were repeatedly heated and cooled at rates of 10 K/h.

Molar magnetic susceptibilities of samples from reaction **III** and **VIII** were recorded with a SQUID magnetometer (MPMS, Quantum Design) in the temperature range 5−310 K at

a magnetic flux density of 0.5 T for sample **III** and 3 T for sample **VIII**. The diamagnetic contributions of the sample holder were subtracted from the data.

The powder samples were cold-pressed into bars whose mass density attains ~85% of the theoretical value calculated from the composition as refined from the single-crystal X-ray data. Thermoelectric properties (electrical resistivity, Seebeck coefficient, thermal conductivity) were simultaneously measured between 2 and 350 K on a commercial system (Thermal transport option, PPMS, Quantum Design). The determination of the absolute values of ρ, S, and λ depends on the sample and contact geometry and is thus inaccurate within ±20%.

For the measurement of thermoelectric properties in the middle temperature range from 323 to 660 K, fine grain and homogeneous powder was hot-pressed in a high-density graphite die at 873 K for approximately 30 min under the pressure of 50 MPa. Rectangular parallelepiped specimens with the approximate dimensions of 2.5 × 2 × 7 mm^3 were cut from the hot-pressed pellets by electric discharge machining for measurements of the Seebeck coefficient and electrical resistivity. Measurements of the Seebeck coefficient and electrical resistivity were made with an ULVAC ZEM-2 apparatus, with measurement errors of less than ±10%. Values of thermal conductivity were estimated from those of thermal diffusivity and specific heat measured by the laser flash method with an ULVAC TC-7000 apparatus for thin-disk specimens with a diameter of 10 mm and a thickness of ~1.2 mm. The value of heat capacity C_p was measured only at room temperature, and we use this value as its heat capacity even above room temperature assuming the Dulong−Petit rule.

Results and Discussions

Synthesis and Phase Analysis. Parallel reactions with different nominal compositions and temperature programs were carried out to explore the phase distribution of the title compounds (Table 1). Under the condition of a slow heating rate of 60 K/h and a long annealing time of 4−5 days, virtually single-phase samples of **CA** and **CB** were obtained from the reaction **III** (nominal composition $Ru_{22.8}Sb_{21.1}Zn_{56.1}$, > 95%) and the reaction **VIII** (nominal composition $Ru_{12}Sb_{11.1}Zn_{76.9}$, > 98%), respectively. The reaction **II** with a nominal composition similar to that of the reaction **III** but with a different temperature program produced only mixed phases. The difference between the purities of the reactions **II** and **III** may be attributed to the fact that the ramping rate in the reaction **III** was so slow that the reaction was almost finished before reaching the boiling point of Zn, while large amount of Zn vaporized in the reaction **II**.

The reaction **V** with a nominal composition between the two compositions of **CA** and **CB** resulted in a mixture. More than 10 crystals were randomly selected from this sample, and their lattice parameters were determined by indexing about 200 reflections from several images collected on single-crystal diffractometer. All these lattice parameters were located in two separated ranges, 24.3−24.4 Å and 25.1−25.2 Å, and these two cubic phases were confirmed by lattice refinements from X-ray diffraction patterns (Figure 1). Two crystals were chosen for further structural characterizations (**CA-s1** and **CB-s1**) by the single-crystal X-ray diffraction methods, and their structures concurred with **CA** and **CB**. All these facts indicated that **CA-s1** (or **CA**) and **CB-s1** (or **CB**) may be two different phases, but we have to preclude the possible phase separation caused by the vaporization of Zn and Sb

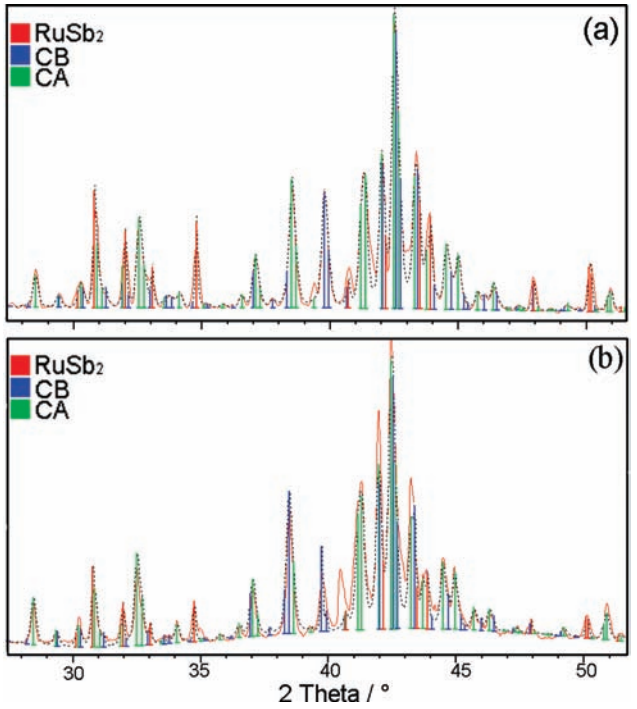

Figure 1. Experimental (red solid curves) powder patterns of reaction **V** (a) and **VI** (b). Black dotted curves were simulated using single crystal data for **CA**, **CB**, and $RuSb_2$. The Bragg positions of these three phases are distinguished by different colors. There is some minor unknown phase in reaction **VI**.

at such a high temperature. Therefore, the reaction **VI** with the same nominal composition with the reaction **V** was tried, but the temperature for homogenizing the elements was decreased from 1273 K in the reaction **V** to 1073 K in the reaction **VI**. The reaction **VI** also generated the mixture of two main phases with lattice parameters in two separated ranges as in the case of the reaction **V** (Figure 1). By all indications, **CA** and **CB** are two distinct phases but not members of an extended solid solution.

Compound **CC** was only obtained in a limited quantity from the reaction **VII** with the nominal composition of $Ru_{12.6}Sb_{11.7}Zn_{75.6}$. The discrepancy between the compositions of **CB** and **CC** is mainly caused by the different atomic ratios of Sb/Zn on the splitting sites. To explore the limit of Sb/Zn, we substantially increased the Sb content in the reaction **IX**, and obtained an almost pure sample (> 90%), from which one crystal (**CD**) was selected and studied by single-crystal X-ray diffraction method. The indexation of the major phase and single-crystal X-ray diffraction indicated that the lattice parameter ranges from 24.3 to 24.4 Å. The results showed that the splitting sites in **CB** and **CC** were replaced by a single exclusively and partially occupied Sb atoms in **CD** (refer to the structural description for details). Therefore, compounds **CB**, **CC**, and **CD** appear to be three compositions of a same solid solution.

Crystal Structures Descriptions. Methods in terms of atomic shells and clusters are used to describe the structures in this work. The structures of the four compounds can be described by two sets of interpenetrating NaCl-type sublattices, with or without glue atoms between them. The first sublattice is decorated by the same rhombicosidodecahedral clusters (the inner four shells of

double-Mackay cluster) but with two distinct orientations, in which the clusters share their square faces. The second one is made up of the same disordered glue clusters but with two distinct orientations, in which the clusters are separated from one another. Because of the geometric similarities between the "structural units" in these four compounds, **CA** is selected as a representative to illustrate the structures. The other three compounds will be mentioned when differences are present. The most prominent differences between these four compounds mainly include the following four aspects: (1) the chemical compositions of the fourth shell (rhombicosidodecahedral shell) in the double-Mackay clusters; (2) the degree of the disorders; (3) the atomic type of the center of the glue cluster, either Ru or Zn; and (4) with or without the glue atoms.

The double-Mackay cluster can be identified in the title compounds. It consists of 127-atom multiple endohedral shells of, from the center outward, a Ru-centered Zn_{12}-icosahedron (Figure 2a), a Zn_{30}-icosidodecahedron (Figure 2b), a larger Ru_{12}-icosahedron (Figure 2c), a 60-atom rhombicosi-dodecahedron (Figure 2d), and the outermost Ru_{12}-icosahedron (Figure 2e). In all four phases as well as the parent phase **HA**, the first inner three shells (55-atom Mackay cluster) and the fifth shell of the

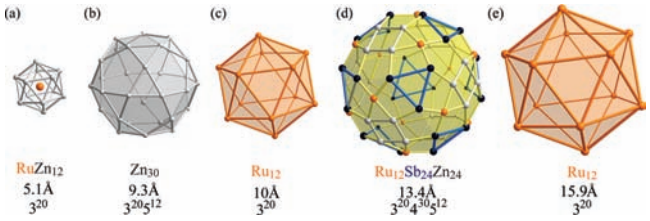

Figure 2. Double-Mackay cluster in the phase **CA**. Shells (a)−(c) form the 55-atoms Mackay cluster $Ru@Zn_{42}Ru_{12}$. (a) Ru centered Zn_{12} icosahedron. (b) Zn_{30} icosidodecahedron. Its pentagons are capped by Ru atoms forming a Ru_{12} icosahedron (c) with diameter similar to the Zn_{30} icosidodecahedron. (d) $Ru_{12}Sb_{24}Zn_{24}$ small rhombicosidodecahedron, the shell next to which, namely, the fifth shell, is the other Ru_{12} icosahedron (e) with vertexes above the pentagons in (d). The orientation of the Ru_{12} icosahedron in (d) differs from that of the icosahedron in the first, third and fifth shells by rotating 90° around the 2-fold axis of the shell in (d). The sizes in the figure are the approximate diameters of the circumsphere of the clusters. As a whole, the diameter of the double-Mackay cluster is ~1.6 nm.

double-Mackay clusters have the same composition, namely, Ru(center)@Zn_{12}@Zn_{30}@Ru_{12} (the symbol "@" in this work denotes that the shells have a common center) and Ru_{12} icosahedron. However, their fourth shells (rhombicosidodecahedron) have different chemical compositions, namely, $Ru_{12}Sb_{24}Zn_{24}$ in **CA**, $Ru_{12}(SbZn)_{24-n}Zn_{24}$ in **CB** and **CC**, $Ru_{12}Sb_{24-n}Zn_{24}$ in **CD**, and Zn_{60} in **HA**. In the fourth shell $Ru_{12}Sb_{24}Zn_{24}$ in the phase **CA**, 24 Sb atoms define the 3-fold rotational symmetry by dispersing 8 Sb_3 triangles in a cubic shape, and 24 Zn atoms define the 4−fold rotational symmetry by dispersing 6 Zn_4 squares in an octahedral shape. Additional 12 Ru atoms form a slightly distorted icosahedron. It is worth noting that the orientation of this distorted Ru_{12} icosahedron coincides with neither that of the smaller icosahedron in the first and the third shell nor that of the larger one in the fifth shell, and it differs from them by rotating 90° around the 2−fold axis of the rhombicosidodecahedron. The six Zn_4 squares in the rhombicosidodecahedral shell are shared by the six neighbors in an octahedral arrangement, and the fifth shell of Ru_{12} icosahedron are formed by atoms from the fourth shell in the six neighboring double-Mackay cluster. So the neighboring double-Mackay clusters interpenetrate into each other in the title compounds, and only the inner four shells of them will be presented in the cluster view of structures for clarity.

In **CA**, the disordered glue clusters are composed of centered Ru atoms and highly disordered Zn aggregates. The Zn atoms in the disordered aggregate partially occupy four distinct sites (64*g* and 3 × 192*j*). Compared with **CA**, the disordered glue clusters in the other three compounds can be described as follows: In **CB**, **CC**, and **CD**, the centered atom is Zn but not Ru, and the zinc aggregate is much less disordered with the sum of about 7.5 Zn atoms (Table 4). The Zn atoms are distributed in the symmetry of a rhombicdodecahedron in all four disordered aggregates (Figure 4, and details in Supporting Information, Figure S2). The matching between the double-Mackay clusters with the 2-fold axis and the disordered glue clusters with the 4-fold axis explains the two distinct orientations of these clusters in the title compounds.

Table 4. Clusters in Complex Alloys in the Ru−Sb−Zn System

shell, polyhedron	**CA**	**CB**	**CC**	**CD**	$Mo_{14}Sn_{24}Zn_{80}$
			Double-Mackay Cluster (0, 0, 0)		
1. Center	Ru	Ru	Ru	Ru	Mo
2. Icosahedron	Zn_{12}	Zn_{12}	Zn_{12}	Zn_{12}	Zn_{12}
3. Icosidodecahedron	Zn_{30}	Zn_{30}	Zn_{30}	Zn_{30}	Zn_{30}
4. Icosohedron	Ru_{12}	Ru_{12}	Ru_{12}	Ru_{12}	Mo_{12}
5. Rhombicosidodecahedron	$Ru_{12}Zn_{24}Sb_{24}$	$Zn_{36}(Zn_{0.36}Sb_{0.5})_{24}$	$Zn_{36}(Zn_{0.73}Sb_{0.25})_{24}$	$Zn_{36}(Sb_{0.71})_{24}$	$Zn_{36}Sn_{24}$
6. Icosohedron	Ru_{12}	Ru_{12}	Ru_{12}	Ru_{12}	Mo_{12}
			Glue Cluster (1/4, 1/4, 1/4)		
1. Center	Ru	Zn	Zn	Zn	Mo
2. Disorder	$Zn_{9.9}$	$Zn_{7.6}$	$Zn_{7.5}$	$Zn_{7.6}$	Zn_{14} (Rhombicdodecahedron)
3. Snub cube	Sb_{24}	$(Zn_{0.36}Sb_{0.5})_{24}Zn_{0.26}$	$(Zn_{0.73}Sb_{0.25})_{24}$	$(Sb_{0.71})_{24}$	Sn_{24}
4. Complex shell	$Ru_{24}Zn_{36}$	Zn_{60}	Zn_{60}	Zn_{60}	Zn_{60}
			Glue Atom		
1. Center	Zn (0, 1/4, 1/4) Ru_4Sb_8	$Zn_{0.026}$ (0.06908, 1/4, 1/4)		$Zn_{0.04}$ (0.069, 1/4, 1/4)	

The glue atoms Zn (0, 1/4, 1/4) in **CA** (the centers of the cyan clusters in Figure 3c) are coordinated by the Sb_8 cube with four capping Ru atoms arranged in the 4−fold rotational symmetry. The glue atoms are closer to the disordered glue clusters in **CB** and **CD**, and finally disappear in **CC** (Figure 4b). In **CB** and **CD**, the glue or interstitial Zn has extremely low occupancy (2.6 and 4%), locating above the square of the snub cube (see details in the next paragraphs) with vertical distance of about 0.8 Å.

Next to the highly disordered Zn aggregate is an Archimedean polyhedron ($3^4.4$), namely, Sb_{24} snub cube (Figures 3b and 5). It is interesting to see that all Sb atoms (192*j*) in the unit cell are exclusively dispersed on the surface of eight snub cubes. These Sb sites are fully occupied in **CA** and partially occupied (SOF = 0.714(6)) in **CD**, but split into two sites occupied by Sb and Zn in **CB** and **CC**, $(Zn_{0.36}Sb_{0.5})_{24}$ and $(Zn_{0.71}Sb_{0.26})_{24}$, respectively. In the four compounds, all the bond lengths between Sb atoms are longer than 3.0 Å. In **CA**, the shortest Sb−Sb contacts are those in Sb_4 squares with value of 3.337 Å and the second shortest Sb−Sb atomic distances < 4 Å are between the atoms from two Sb_4 squares on the same snub cube (3.914 Å) and atoms from two neighboring snub cubes (3.820 Å). From **CB**, **CD**, to **CC**, these snub cubes shrink gradually, and the shortest distances between snub cubes are larger than 4.4 Å.

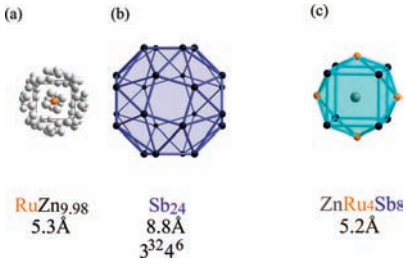

Figure 3. In the **CA** phase, disordered glue cluster (a) is disordered zinc aggregate with a rhombic dodecahedron symmetry and a Ru center, the shell next to which is a Sb_{24} snub cube (b). The glue atom Zn is coordinated by a capped cubic Ru_4Sb_8 (c).

In snub cube, the Sb−Sb bond lengths in **CB** range from 3.367 to 3.431 Å, from 3.321 to 3.368 Å in **CD**, and from 3.093 to 3.319 Å in **CC**. Various Sb−Sb interactions have strong influence on the size of band gaps, in turn, on their thermoelectric properties.[23,24] In reported antimonides, Sb atom substructures vary from molecular Sb units to infinite chains, layers, and three-dimensional networks.[23,25] Here, these $(Sb_{1-\delta}Zn_\delta)_{24}$ snub cubes are either connected in **CA** or discrete in **CB**, **CC**, and **CD**, which is not found in other antimonides. The influence of the change in Sb−Sb interactions on their thermoelectric properties is significant, as will be discussed in the part of transport properties later.

All four compounds include structural motifs similar to that in $Mo_7Sn_{12}Zn_{40}$ (Table 4).[13] Except for the chemical composition, the most prominent difference between them is that there is no disorder in $Mo_7Sn_{12}Zn_{40}$, in which the first shell inside the snub cube is a rhombicdodecahedron $Mo@Zn_{14}$, while a highly disordered zinc aggregate in the four title compounds. The $(Sb_{1-\delta}Zn_\delta)_{24}$ snub cube filled with highly disordered zinc aggregates resembles cage structures in clathrate or skutterudite compounds. Cages in clathrate compounds, such as 24-atom tetrakaidecahedron and 20-atom pentagonal dodecahedron, encapsulate weakly bound guest atoms that can scatter short-wavelength phonons so as to reduce lattice thermal conductivity effectively. Although Sb-based clathrate compounds are expected to exhibit lower thermal conductivity than Si, Ge, or Sn-based calthrate compounds because Sb is heavier than Group 14 elements, no Sb-based clathrates have been reported so far except for the type-I clathrate compound $Cs_8M_{18}Sb_{28}$ (M = Zn, Sb).[26] Here, the $(Sb_{1-\delta}Zn_\delta)_{24}$ snub cubes filled with highly disordered zinc aggregates are assumed to scatter longer wavelength phonons because of their larger size than the guest atoms in clathrate or skutterudite compounds. Together with atomic substitution sites, phonons in a broader range of wavelength may be expected to be scattered effectively.

Relationship to Quasicrystal. The title compounds show some common structural and electronic features as seen in QC or quasicrystal approximants[27] as follows:

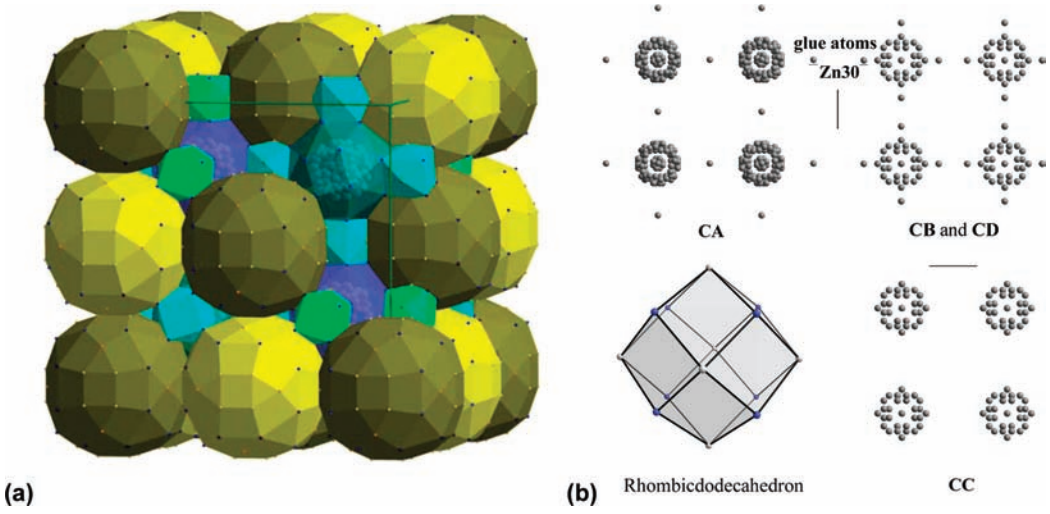

Figure 4. Panel (a) shows the packing of rhombicosidodecahedral clusters (all the four shells in Figure 2), disordered glue clusters (the two shells in Figures 3a and 3b) and glue atoms (Figure 3c) in **CA**. Two distinct orientations of the clusters are indicated by dark and light colors. Four clusters at one corner are omitted for clarity. Green lines are the cubic unit cell. The glue atoms Zn30 (the centers of the cyan clusters) are fully occupied in **CA**, while they appear in **CB** and **CD** as atoms with extremely low occupancies and are closer to the glue clusters, and there is not glue atom in **CC** (panel b). This disordered clusters show the symmetry of a rhombic dodecahedron (the left bottom in panel b) which consists of one cubic (blue atoms) and one octahedron (gray atoms).

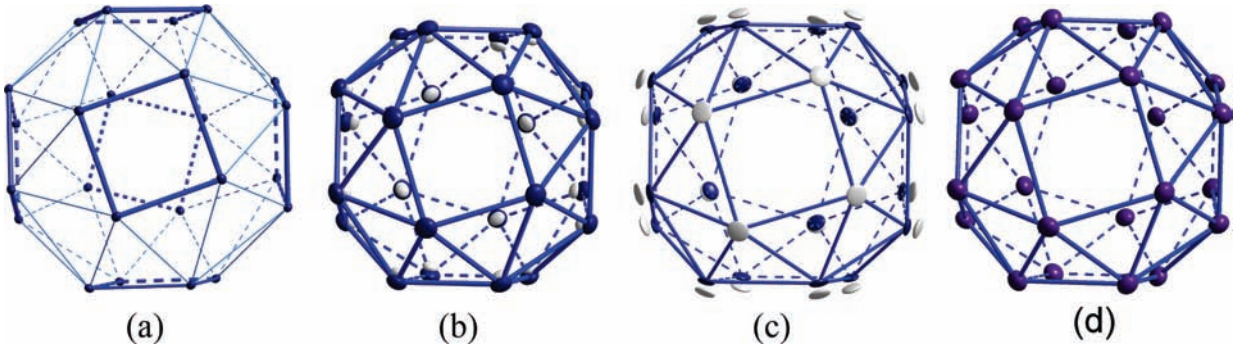

Figure 5. All Sb atoms (192*j*) disperse on $(Sb_{1-\delta}Zn_{\delta})_{24}$ snub cubes, in which no Sb−Sb bond with bond length less than 3.0 Å was found. The bold blue lines mean weak bonds between Sb atoms. In the Sb_{24} in **CA** (a), six Sb_4 squares are distributed perpendicular to the 4-fold axis. All sites split into two sites in **CB** (b) and **CC** (c), $(Sb_{0.5}Zn_{0.36})_{24}$ and $(Sb_{0.25}Zn_{0.73})_{24}$, respectively. Only partially occupied Sb atoms with SOF = 0.714 exist in **CD**. Thermal ellipsoids are at 50% probability level. Dark blue, Sb; gray, Zn.

(1) Mackay-type clusters are usually formed in systems consisting of transition-metal and main-group elements on the right side of the periodic table, such as Al−Pd−Me (Me = Mn, Re, Ru, Os), Al−Cu−Me (Me = Fe, Ru, Os), Ti−Zr−Ni.[10] So do the title compounds. In all four compounds, most of the atoms in the unit cell can be covered by the double-Mackay clusters with icosahedral symmetry, 88% in **CA**, 92.2% in **CB**, 92.3% in **CC**, and 92.8% in **CD**. The remaining atoms (highly disordered Zn aggregate and glue atoms) fill the interspaces between the double-Mackay clusters.

(2) The valence electron concentration (e/a) is confirmed as the dominant factor of stabilizing QCs.[28] All three types of icosahedral QC (*i*-QC) have restricted ranges of e/a, approximately 1.75 for the Mackay-type, about 2.1−2.2 for the Bergman-type, and close to 2.0 for the Tsai-type.[28] The e/a are 1.58 and 1.77 for **CA** and **CB**, respectively, if negative valency −2.66 is assigned to the Ru atom.[29] Their e/a values, especially that of **CB**, are close to the favorable value for Mackay-type *i*-QC. By substituting Sb with Sn in phase **CA**, the tolerance of the substitution concentration exceeds 30 at.% of Sb, which suggests the electron concentration can be varied by changing the composition. Therefore, the requirement on the e/a value for the formation of QCs (if this is the case) for the title compounds might be achieved by the Sn substitution.

(3) Figure 6 shows the temperature dependence of electrical resistivity (ρ) for **CA**, indicating a semiconductor-like behavior. The inset in Figure 6 shows a logarithm of electrical resistivity plotted against inverse temperature. The band gap energy E_g estimated from the slope $E_g/2k_B$ of the linear fit,

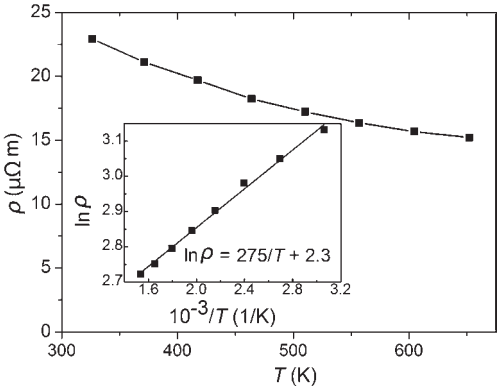

Figure 6. Temperature dependence of the electrical resistivity ρ of **CA**. The insets indicate the ln $\rho-1/T$ plot. In the inset, the solid line represents the result of fitting by each equation on the graph.

where k_B is the Boltzmann constant, is 0.047 eV. This small value of E_g resembles the feature of the pseudogap near E_F that usually appears in QCs and quasicrystal approximants.[30]

Nevertheless, the title compounds are not favorable for icosahedral quasicrystal approximants from the viewpoint of symmetry relationship. The title compounds crystallize in the space group of $Fm\bar{3}c$, which is not within the subgroups of $m\bar{3}5$ in *i*-QCs.[31]

Magnetic Properties and Thermal Stability. The relatively small temperature-independent molar magnetic susceptibilities, **CA** (-11.3×10^{-11} m^3 mol^{-1}) and **CB** (-14.9×10^{-11} m^3 mol^{-1}) over 2−300 K (Supporting Information, Figure S3), indicate that they are both diamagnetic. **CA** and **CB** are stable up to 1200 and 1029 K with increasing temperature, respectively, exhibiting a quite large difference of ~170 K (Supporting Information, Figure S4). Above their maximum stable temperatures, both **CA** and **CB** melted. The powder X-ray diffraction pattern performed at ambient temperature on the sample of **CA** rapidly quenched from 1273 K was different with the sample without heat treatment, while

(23) Kleinke, H. *Chem. Soc. Rev.* **2000**, *29*, 411.
(24) Xu, J. X.; Kleinke, H. *J. Comput. Chem.* **2008**, *29*, 2134.
(25) Papoian., G. A.; Hoffmann., R. *Angew. Chem., Int. Ed.* **2000**, *39*, 2408.
(26) Liu, Y.; Wu, L. M.; Li, L. H.; Du, S. W.; Corbett, J. D.; Chen, L. *Angew. Chem., Int. Ed.* **2009**, *48*, 5305.
(27) Goldman, A. I.; Kelton, R. F. *Rev. Mod. Phys.* **1993**, *65*, 213.
(28) Tsai, A. P. In *Physical Properties of Quasicrystals*; Stadnik, Z. M., Ed.; Springer: New York, 1999; p 5.
(29) Tsai, A. P. *J. Non-Cryst. Solids* **2004**, *334*−*335*, 317.
(30) (a) Pierce, F. S.; Poon, S. J.; Biggs, B. D. *Phys. Rev. Lett.* **1993**, *70*, 3919. (b) Smith, A. P.; Aschcroft, N. W. *Phys. Rev. Lett.* **1987**, *59*, 1365.
(31) Lin, Q. S.; Corbett, J. D. Controlled Assembly and Modification of Inorganic System. In *Structure & Bonding*; Mingos, D. M. P., Ed.; Springer: Berlin/Heidelberg, 2009; Vol. *133*, p 1.

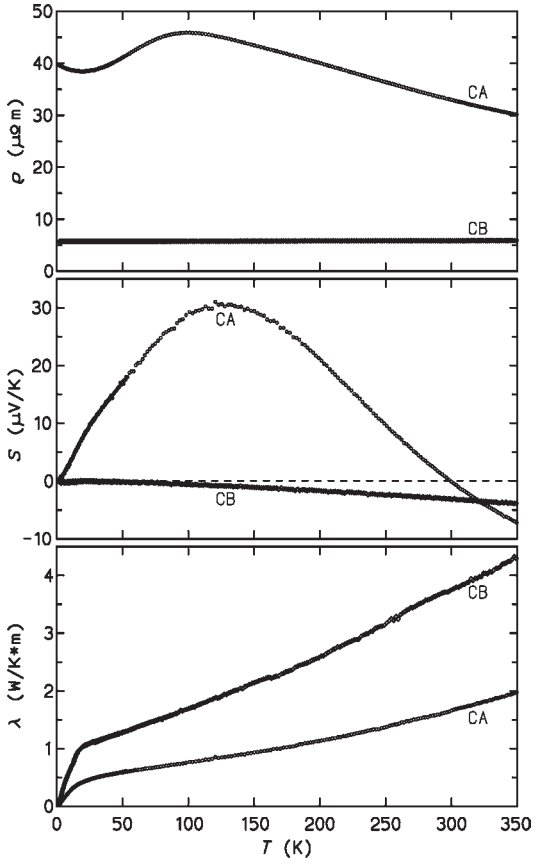

Figure 7. Electrical resistivity (a), thermopower (b), and thermal conductivity (c) of **CA** and **CB** in the low temperature down to 2 K.

that of the sample of **CB** rapidly quenched from 1173 K almost remained unchanged.

Thermoelectric Properties. To get an idea of the potential thermoelectric properties of these as-produced samples, measurements of their charge and heat transport properties have been made. Figure 7 compiles the electrical resistivity ρ, the Seebeck coefficient S (thermopower), and the thermal conductivity λ of **CA** and **CB** in the temperature range from 2 to 350 K. The two compounds display remarkable differences in all three properties.

The resistivity of **CB** is very weakly dependent on temperature: $\rho(T)$ increases only from 5.69 $\mu\Omega$ m at 21 K to 5.84 $\mu\Omega$ m at 300 K. Below 20 K a weak rise of $\rho(T)$ toward lower temperatures is observed. The temperature dependence of $\rho(T)$ of **CA** is complex: starting from $T = 2$ K, $\rho(T)$ decreases slightly (similar to that for **CB**) and reaches a local minimum at $\approx$20 K. Then it increases to a maximum of 46 $\mu\Omega$ m at $\approx$100 K and finally decreases continuously with increasing temperature (ρ(300 K) = 33 $\mu\Omega$ m). According to single crystal X-ray diffraction data, no phase transition took place above 92 K for **CA** (low temperature limitation in our lab). As expected for complex alloys, the magnitude of the electrical resistivity of the investigated compounds is well above $\sim$1 $\mu\Omega$ m (Ioffe−Regel limit[32]). Both crystal structures contain highly disordered clusters leading to high residual resistivities. The resistivity of **CA** is, however, 5−8 times higher than that of **CB** which may be partially due to the larger disorder in the zinc aggregates of the former compound. While ρ of **CA** is of the order typical for a heavily doped semiconductor, the magnitude of ρ of **CB** is more characteristic of a bad metallic conductor. In the middle temperature range from 323 to $\sim$660 K, the resistivities for the hot-pressed specimens of both **CA** and **CB** continue the tendencies at low temperatures (Supporting Information, Figure S5).

The Seebeck coefficient $S(T)$ of **CB** is small and negative, and its absolute value increases continuously with increasing temperature (S(660 K) = -8.6 μV K^{-1}). Thus, the compound is typically metallic, and electrons are the (majority) charge carriers. As could be guessed from the resistivity data, $S(T)$ of **CA** is more complex. It increases from zero almost linearly with increasing temperature until it reaches a maximum of $+31$ μV K^{-1} at 130 K. Above this temperature S decreases, and a change of sign occurs at room temperature (299 K), then $S(T)$ decreases to -25.6 μV K^{-1} at 660 K. The complicated behavior of resistivity and thermopower is thus connected to the multiband conduction mechanism and changes in the concentration or the mobility of the different charge carriers in this compound.

The thermal conductivity $\lambda(T)$ of both compounds increases generally with temperature. Below $\sim$20 K a steep increase (with a limiting power law $\lambda \propto T^{\alpha}$ much weaker than for crystalline materials; $\alpha \leq 1.7$) is observed. The rise is cutoff and no phonon peak (as for crystalline materials) is observed. At elevated temperatures $\lambda(T)$ increases almost linearly with temperature. Above 100 K an anomalous increase of $\lambda(T)$ is due to heat radiation loss which is proportional to T^3. The thermal conductivity of **CA** is much smaller than that of **CB**, which was expected from the fact that the zinc aggregates in the former structure are more disordered. Taking into account the heat radiation loss, the value of λ for **CA** can be estimated to be around 1.3 W m^{-1} K^{-1} at room temperature. The thermal conductivity of hot-pressed samples of **CB** at room temperature is $\sim$0.9 W m^{-1} K^{-1}, which is smaller than that of cold−pressed samples by $\sim$30% (Figure 7). Such a value is typically associated with glass-like materials, for example, λ of vitreous silica is around 1.5 W m^{-1} K^{-1} at 300 K.[33] For **CB** a value λ(300 K) of 3.2 W m^{-1} K^{-1} can be estimated.

Conclusions

In this work we obtained four new cluster-based complex alloys ruthenium zinc antimonides with large unit cells. By all indications, compounds **CA** and **CB** are distinct phases, while compounds **CB**, **CC**, and **CD** are three members of a same solid solution. In all four compounds, novel $(Sb_{1-\delta}Zn_{\delta})_{24}$ snub cubes filled with highly disordered zinc aggregates are observed, and these snub cubes with different chemical compositions are either weakly interacted or isolated. These snub cube substructures resemble the cage structures in clathrate or skutterudite compounds, but are more disordered and larger in size (about 5.3 Å in diameter in **CA**). Together with substituted atomic sites in doped rigid double-Mackay clusters, they are expected to scatter phonons in a broader range of wavelength and be more effective in reducing thermal conductivity. Transport property measurements of compounds **CA** and **CB** reveal that the compounds exhibit reasonably good electrical conductivity and rather low thermal

(32) Ioffe, A. F.; Regel, A. P. *Prog. Semicond.* **1960**, *4*, 237.

(33) Damon, D. H. *Phys. Rev. B* **1973**, *8*, 5860.

conductivity simultaneously. The Seebeck coefficients are unfortunately moderate. Approaches, like appropriate chemical substitution and the application of spark plasma sintering (SPS), and so forth[34] may be worthwhile exploring to improve the physical properties. The structural model, rigid clusters with inherent disordered glue clusters, is expected to be extended to other systems by isoelectronic replacements or introduction of other rigid icosahedral clusters.

Acknowledgment. Fruitful discussion with Prof. Bernd Harbrecht and his great support on experiments are gratefully acknowledged. The authors thank Clemens Pietzonka for magnetic susceptibility measurement. D.-B.X. thanks the Alexander von Humboldt Foundation (Germany) and Japan Society for the Promotion of Science (JSPS) for postdoctoral fellowships.

(34) Takagiwa, Y.; Kamimura, T.; Hosoi, S.; Okada, J. T.; Kimura, K. *Z. Kristallogr.* **2009**, *224*, 79.

Supporting Information Available: Table S1−2 (data collection, crystallographic data, and atomic coordinates for **CA-s1**, **CB-s1** and **CB-s2**), Figures S1−S5 (powder X-ray diffraction patterns, DTA, magnetic susceptibilities, and thermoelectric properties at middle temperature range), and X-ray crystallographic data (CIF). This material is available free of charge via the Internet at http://pubs.acs.org.